Atmospheric Emitted Radiance Interferometer. Part II: Instrument Performance

R. O. KNUTESON, H. E. REVERCOMB, F. A. BEST, N. C. CIGANOVICH, R. G. DEDECKER, T. P. DIRKX, S. C. ELLINGTON, W. F. FELTZ, R. K. GARCIA, H. B. HOWELL, W. L. SMITH, J. F. SHORT, AND D. C. TOBIN

Space Science and Engineering Center, University of Wisconsin—Madison, Madison, Wisconsin

(Manuscript received 8 January 2004, in final form 20 May 2004)

ABSTRACT

The Atmospheric Emitted Radiance Interferometer (AERI) instrument was developed for the Department of Energy (DOE) Atmospheric Radiation Measurement (ARM) Program by the University of Wisconsin Space Science and Engineering Center (UW-SSEC). The infrared emission spectra measured by the instrument have the sensitivity and absolute accuracy needed for atmospheric remote sensing and climate studies. The instrument design is described in a companion paper. This paper describes in detail the measured performance characteristics of the AERI instruments built for the ARM Program. In particular, the AERI systems achieve an absolute radiometric calibration of better than 1% (3σ) of ambient radiance, with a reproducibility of better than 0.2%. The knowledge of the AERI spectral calibration is better than 1.5 ppm (1σ) in the wavenumber range 400–3000 cm^{-1}.

1. Introduction

One of the key instruments supported by the U.S. Department of Energy (DOE) Atmospheric Radiation Measurement (ARM) instrument development program was the Atmospheric Emitted Radiance Interferometer (AERI) (Stokes and Schwartz 1994). The AERI instrument measures the downwelling atmospheric emission spectrum at the surface with high spectral resolution and high absolute accuracy. The design of the AERI instrument meeting the requirements of the ARM Program is described in a companion paper (Knuteson et al. 2004, hereafter referred to as Part I). All the AERI systems built by the University of Wisconsin Space Science and Engineering Center (UW-SSEC) for the ARM Program include custom data processing software used to produce calibrated radiance spectra in real time. A description of the real-time data processing flow used in the AERI system is provided in Minnett et al. (2001). In this paper, the authors describe the algorithms used in the real-time data processing to achieve the desired radiometric performance. The actual performance achieved by the various AERI instruments built at UW-SSEC is presented, along with appropriate calibration verification data.

Corresponding author address: Dr. Robert O. Knuteson, Space Science and Engineering Center, University of Wisconsin—Madison, 1225 West Dayton St., Madison, WI 53706.
E-mail: robert.knuteson@ssec.wisc.edu

2. AERI performance

The AERI is a ground-based Fourier transform spectrometer (FTS) for the measurement of atmospheric downwelling infrared thermal emission at the earth's surface. As described in Part I, the AERI instrument was built as an operational facility instrument for the ARM Program for the routine measurement of downwelling infrared radiance to better than 1% absolute accuracy. This section summarizes the detailed performance characteristics of each of the eight AERI instruments built for the ARM Program based upon laboratory tests and clear-sky intercomparisons performed at UW-SSEC prior to the delivery of each instrument. The details presented here represent the AERI instrument performance at the time of initial deployment into the ARM field network. A characterization of the data record of field observations of the AERI instruments within the ARM network is deferred to a future paper.

a. Radiometric performance

This section describes how the performance of the AERI systems meets the requirements listed in Part I for the production of calibrated infrared radiance spectra. The AERI real-time data processing applications convert the raw interferometer data to calibrated radiances by implementing a sequence of operations including 1) correction for detector nonlinearity in the longwave band, 2) radiometric calibration using the onboard reference blackbodies, 3) correction for spectral line shape effects, and 4) resampling of the radiance spectra to a common wavenumber grid. Details of the

AERI data processing algorithms are presented in the following sections on system linearity, radiometric calibration, spectral coverage and instrument line shape, wavenumber calibration, noise, and reproducibility.

1) NONLINEARITY CORRECTION

The AERI system uses a mercury cadmium telluride (HgCdTe) and indium antimonide (InSb) detector package. Each detector uses separate preamplifiers, which are linear by design. The InSb detector response is inherently linear; however, the HgCdTe detector response is known to exhibit nonlinear behavior. The system linearity of the longwave detector band has been characterized in each of the AERI systems using reference observations at +60°C (hot), +20°C (ambient), and near 77 K (cold). The size of the nonlinearity effect in the calibrated AERI longwave radiance is relatively small (order 1%–2% of ambient radiance), but the absolute calibration requirement of ''better than 1% of ambient radiance'' for all scene conditions implies that a nonlinearity correction is necessary. The goal has been to characterize the nonlinearity of each longwave detector to better than 10%, which, when that knowledge is applied as a nonlinearity correction, implies an uncertainty contribution to the final calibrated radiance of less than about 0.2% of ambient radiance.

UW-SSEC has developed a correction formulation using a physical model for the known quadratic and cubic dependencies of the nonlinearity of photoconductive HgCdTe detectors. Only the quadratic nonlinearity term is described here. The cubic term was determined to be unnecessary at the relatively low flux levels used in the AERI application. The signal at the detector is modeled as the measured interferogram plus a dc level offset from zero. The corrected complex spectra for hot, ambient, and cold (LN2) scenes is given by the equation

$$C_{\text{corr}}^{H,A,C} = C_m^{H,A,C} + a_2\text{FT}\{(I_m^{H,A,C} + V_m^{H,A,C})^2\}$$

$$C_{\text{corr}}^{H,A,C} = C_m^{H,A,C}(1 + 2a_2V_m^{H,A,C}) + a_2\text{FT}\{(I_m^{H,A,C})^2\}, \quad (1)$$

where I_m is the measured interferogram, C_m is the Fourier transform of the measured interferogram, V_m is the modeled dc offset, and a_2 is the quadratic nonlinearity coefficient. The symbol FT{ } represents the Fourier transform of the argument. Note that the dominant correction term is proportional to the measured complex spectrum itself because the squared interferogram has only a small contribution in-band. In fact, the main out-of-band contribution of the squared interferogram is used to determine the value of the a_2 parameter. Since the dc level is not measured directly in the AERI instruments, an empirical model was developed to account for level variations caused by different scene flux levels. The dc-level model is a linear function of the integrated scene flux with an offset proportional to the integrated flux obtained when viewing a liquid nitrogen reference blackbody in the laboratory prior to deployment. A real-time correction is made to account for instrument background flux differences between the laboratory characterization at UW-SSEC prior to deployment and the actual interferometer operating environment. The model parameterizes the instrument background flux and interferometer modulation efficiency, but the final calibration correction is relatively insensitive to the absolute value of these quantities since the calibration equation cancels any offsets and multiplicative factors common to the scene and calibration views. The dc-level model used in the routine processing of AERI data is defined as

$$V_{\text{dc}} = -\left[\frac{1}{\text{MF}}\right]\{(2 + f_{\text{back}})[-I_H(0) + I_H^{\text{lab}}(0) - I_C^{\text{lab}}(0)] + I(0)\}, \quad (2)$$

where MF is the modulation efficiency (fixed at a value of 0.7), f_{back} is the fraction of background radiation (fixed factor of 1.0), $I(0)$ is the value of the interferogram at zero path difference (ZPD) for the current scene, $I_H(0)$ is the most recent hot blackbody value (used to track instrument temperature changes), and $I_H^{\text{lab}}(0)$ and $I_C^{\text{lab}}(0)$ are values of the hot and LN2 blackbody determined in the laboratory prior to instrument deployment. An algorithm based Eqs. (1) and (2) is used to perform a real-time nonlinearity correction of the AERI calibration and scene views prior to the radiometric calibration of each scene.

The methodology used to determine the quadratic nonlinearity coefficient, a_2, is briefly described here. A special nonlinearity test is a part of the AERI instrument calibration procedure performed at UW-SSEC. The AERI system is made to cycle through views of the internal hot and ambient blackbodies and a nadir view of a cavity submerged 4 in. below the surface of a liquid nitrogen bath. A 4-h test is required to collect about 120 mean spectra (120 × 46 interferometer scans) in each Michelson mirror sweep direction for each of the three reference targets. The 4-h test duration is needed to reduce the noise sufficiently in the out-of-band region to extract the small nonlinearity signature. The test data are used in a fit to the equation $\Re_{\text{corr}}^{HA} = \Re_{\text{corr}}^{AC}$, which forces the real part of the instrument system responsivity (or gain) computed from the hot and ambient temperature references to agree with that computed from the ambient and LN2 reference targets after nonlinearity correction. Using the expansion given in Eq. 1, the difference in measured responsivities between a hot–ambient and ambient–cold calibration can be written as

$$\Re_m^{H,A} - \Re_m^{A,C} = a_2\left\{\frac{(\text{FFT}[(I_m^H + V_m^H)^2] - \text{FFT}[(I_m^A + V_m^A)^2])}{(\hat{B}_\upsilon^H - \hat{B}_\upsilon^A)} - \frac{(\text{FFT}[(I_m^A + V_m^A)^2] - \text{FFT}[(I_m^C + V_m^C)^2])}{(\hat{B}_\upsilon^A - \hat{B}_\upsilon^C)}\right\}. \quad (3)$$

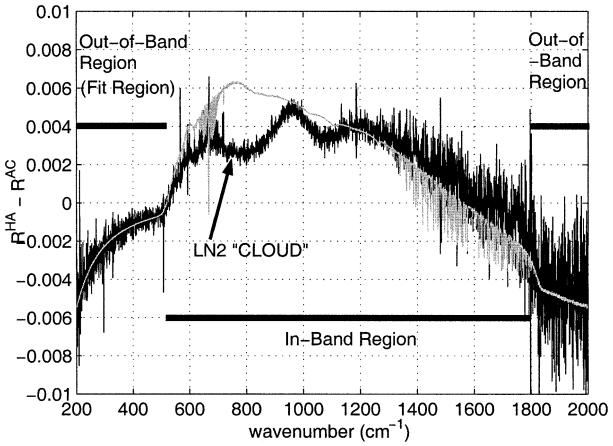

FIG. 1. The nonlinearity model fit (gray curve) to a measured responsivity difference between hot/ambient and ambient/LN2 reference targets. The fit region is 200–460 cm^{-1}, which avoids the ''in-band'' uncertainties of the LN2 target emissivity due to a liquid water cloud that forms over the cold target. Note that the quadratic nonlinearity model agrees in both the 200–460- and 1800–2000-cm^{-1} out-of-band regions even though the least squares fit only uses the first region to determine a_2. The test data are of AERI-05 on 8 Dec 1998 but are typical of all standard AERI systems. Units are instrument counts per radiance unit {counts per [mW (m^2 sr cm^{-1})$^{-1}$]}.

While, in principle, both the in-band and out-of-band responsivity could be used to determine the nonlinearity coefficient, a_2, in practice the uncertainty of the spectral emissivity of the LN2 cold blackbody is too large to allow the use of an in-band fit. Fortunately, the out-of-band signal for the quadratic nonlinearity provides an unambiguous determination of a_2, largely independent of the issues that affect the in-band signal. Figure 1 shows a least squares regression fit for a_2 to the difference of measured responsivities in the 200–460 cm^{-1} region using Eq. (3) to determine the quadratic nonlinearity coefficient. The large difference between the measured and modeled results between 700 and 1000 cm^{-1} is due to the absorption caused by the liquid water cloud (fog) that forms over the open-mouth LN2 dewar. For this and other reasons, a liquid nitrogen cold target does not make a suitable operational calibration reference. For the UW-SSEC AERI systems, the LN2 reference is used only in the determination of the instrument nonlinearity in the out-of-band region, which is relatively immune to the uncertainty in emissivity that impacts the in-band region.

The nonlinearity determined for each of the longwave detectors used in the AERI instruments is summarized in Table 1. The in-band nonlinearity correction factor, $2a_2V_{dc}$, was computed using the a_2 value measured on the stated test date and dc-level values computed from Eq. (2) using $I(0)$ equal $I_H(0)$, zero, and $I_C(0)$ to represent the hot, ambient, and LN2 blackbodies, respectively. These dc-level values span the range of nonlinearity corrections used in the calibration of atmospheric scenes. The nonlinearity corrections (as a percent of raw signal) vary from 1%–2% for the AERI-01 at the Southern Great Plains (SGP) Central Facility (CF) to 3%–6% for the Tropical Western Pacific (TWP) systems. Since the radiometric calibration is based on differences from the ambient blackbody, the effective correction is generally less than 2% of the ambient blackbody radiance. An example of an AERI nonlinearity correction is shown in Fig. 2 for the AERI-05 (Hillsboro) system. Figure 2 shows that the nonlinearity correction is important for the AERI system because the correction is of the same order of magnitude as the 1% absolute calibration specification.

TABLE 1. Estimate of the ''in-band'' nonlinearity correction for each of the AERI longwave detectors as a percent of the raw signal ($100 \times 2a_2V_{dc}$) for the hot (333 K), ambient (300 K), and LN2 (77 K) blackbodies. The extended-range AERI detectors for the NSA site do not exhibit a measurable nonlinearity, and no nonlinearity correction is applied. The systems labeled ''MAERI'' are the three Marine-AERI systems built by UW-SSEC for the University of Miami, described in Minnett et al. (2001).

Instrument	Lab test date	HBB (%)	ABB (%)	LN2 (%)
AERI-00	16 Sep 1997	1.5	1.3	0.9
AERI-01	10 Jun 1997	1.6	1.4	0.9
AERI-00U	N/A	0.0	0.0	0.0
AERI-02	10 Nov 1998	4.5	3.8	2.5
AERI-03	11 Nov 1998	4.9	4.1	2.7
AERI-04	8 Dec 1998	1.2	1.0	0.7
AERI-05	8 Dec 1998	2.6	2.2	1.5
AERI-06	4 May 2001	4.7	3.9	2.6
AERI-07	N/A	0.0	0.0	0.0
AERI-08	24 May 2000	5.9	5.0	3.4
MAERI-01	3 Dec 1998	5.2	4.5	3.0
MAERI-02	1 Sep 1997	8.1	6.7	4.5
MAERI-03	2 Sep 1998	8.0	6.8	4.5

2) RADIOMETRIC CALIBRATION

This section describes the methodology and error analysis associated with radiometric calibration and verification of the AERI instruments.

(i) Methodology

The AERI instruments are configured to operate on a repeating scene mirror schedule such that the scene being calibrated is bracketed by views of the onboard reference blackbodies. The standard AERI scene mirror schedule is a repeating sequence of the form HASAHS, where *H, A,* and *S* represent views to the hot blackbody, ambient blackbody, and sky positions, respectively. Multiple *S* views are also possible, with a practical limit imposed by the rate of drift of instrument temperatures during the calibration period. The standard view angles and dwell times for each mirror position are given in Table 2 for the AERI-01 system. There are two Michelson mirror sweeps (forward and backward) for each total scan. Dwell times in Table 2 are only approximate. The AERI calibration methodology is to define a calibration sequence composed of the scene view to be calibrated and the pair of hot and ambient blackbody

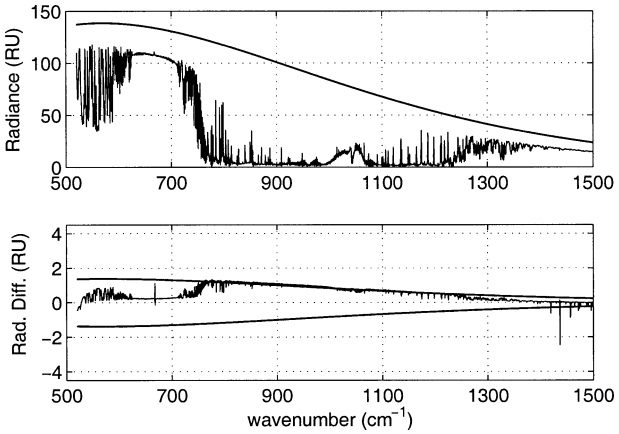

FIG. 2. This example shows the magnitude of the nonlinearity correction for calibrated radiances on a typical clear-sky observation. The observation was made using AERI-05 at UW–Madison on 7 Dec 1998. (top) An overlay of the calibrated longwave spectrum and a Planck function at the ambient blackbody temperature (290 K). (bottom) A radiance difference of the calibrated spectrum with and without a nonlinearity correction. The solid lines indicate ±1% of the ambient blackbody radiance. [Radiance units: RU = mW (m^2 sr cm^{-1})$^{-1}$.]

views measured closest in time before and after each scene view. In order to account for changes in the instrument temperature during a calibration sequence, the blackbody temperature measurements are fit to a linear function of time, and this fit is evaluated at the center time of the sky view measurements. A similar linear interpolation to the sky view time is performed for each complex spectral element of the hot blackbody and ambient blackbodies.

Following Revercomb et al. (1988), the equation used in the radiometric calibration of the AERI systems is

$$N_\upsilon = \mathrm{Re}\left\{\frac{C_\upsilon^S - C_\upsilon^A}{C_\upsilon^H - C_\upsilon^A}\right\}(\hat{B}_\upsilon^H - \hat{B}_\upsilon^A) + \hat{B}_\upsilon^A,$$

$$\hat{B}_\upsilon^H = e_\upsilon^H B_\upsilon(T^H) + (1 - e_\upsilon^H)B_\upsilon(T^R),$$

$$\hat{B}_\upsilon^A = e_\upsilon^A B_\upsilon(T^A) + (1 - e_\upsilon^A)B_\upsilon(T^R), \qquad (4)$$

where N_υ is the calibrated radiance for the spectral element at wavenumber υ; Re{ } refers to the real part of the complex argument; and the labels *S*, *H*, *A* refer to the sky, hot blackbody, and ambient blackbody scenes, respectively. The variables C_υ, e_υ, and B_υ refer to the observed complex spectra, the blackbody emissivity spectra, and the Planck function radiance at temperature *T*, respectively. The variable T^R is the ''reflected'' temperature, that is, the radiative temperature of the environment that can emit into the blackbody cavity. The AERI software uses the blackbody support structure temperature as an estimate of the reflected temperature. The forward and backward Michelson mirror sweeps are calibrated separately using Eq. (4), and the calibrated radiances for each sweep direction are averaged together to create the mean calibrated radiance corresponding to an individual sky dwell period. Any complex offset or phase associated with the warm instrument emission is cancelled in the ratio of complex difference spectra contained in Eq. (4). In fact, the quantity

$$D_\upsilon = \mathrm{Im}\left\{\frac{C_\upsilon^S - C_\upsilon^A}{C_\upsilon^H - C_\upsilon^A}\right\}(\hat{B}_\upsilon^H - \hat{B}_\upsilon^A) \qquad (5)$$

where Im{ } refers to the imaginary part of the complex argument, is zero within the instrument noise. The quantity D_υ is used in the AERI real-time quality assessment as an estimate of the noise on the observed scene. Another useful diagnostic of the AERI system radiometric performance is the instrument system responsivity defined to be the inverse of the slope of the linear calibration equation

$$\Re_\upsilon = \frac{C_\upsilon^H - C_\upsilon^A}{\hat{B}_\upsilon^H - \hat{B}_\upsilon^A}. \qquad (6)$$

The system responsivity is a measure of the instrument response (or gain) per unit radiance input as a function of wavenumber. The responsivity magnitude is sensitive to the instrument optical transmission, the detector responsivity, and the detector preamp gain settings. Figure 3 shows the responsivity spectrum and the corresponding calibrated radiances for an example spectrum. The difference of the hot and ambient views in Eq. (6) removes the instrument emission so that to first order the magnitude of the system responsivity is independent of instrument temperature. The stability of the system responsivity over time is a valuable diagnostic of instrument performance.

TABLE 2. Scene mirror sequence for the AERI-01 system.

Label	Angle (°)	No. total scans	Dwell (s)
H	299.21	23	100
A	58.35	23	100
S	0	45	200
A	58.35	23	100
H	299.21	23	100

(ii) Predicted calibration performance

A differential error analysis of the calibration equation was used to guide the instrument development of the AERI system. In particular, the accuracy of the reference blackbodies was chosen to ensure that the instrument measurements that enter into the calibration equation are adequate to meet the overall calibration requirements. If N_υ represents the calibrated radiance for a set of known blackbody temperature and emissivity values, then Eq. (4) can be used to write an equation for the radiance derived for a set of perturbed blackbody parameters. One can then compute the radiance perturbation $\Delta N_\upsilon = N_\upsilon' - N_\upsilon$ for a range of scene temperatures by perturbing each parameter. Figure 4 shows the radiance errors as a percent of ambient blackbody radiance for the uncertainty estimates given in Table 3. Figure 4

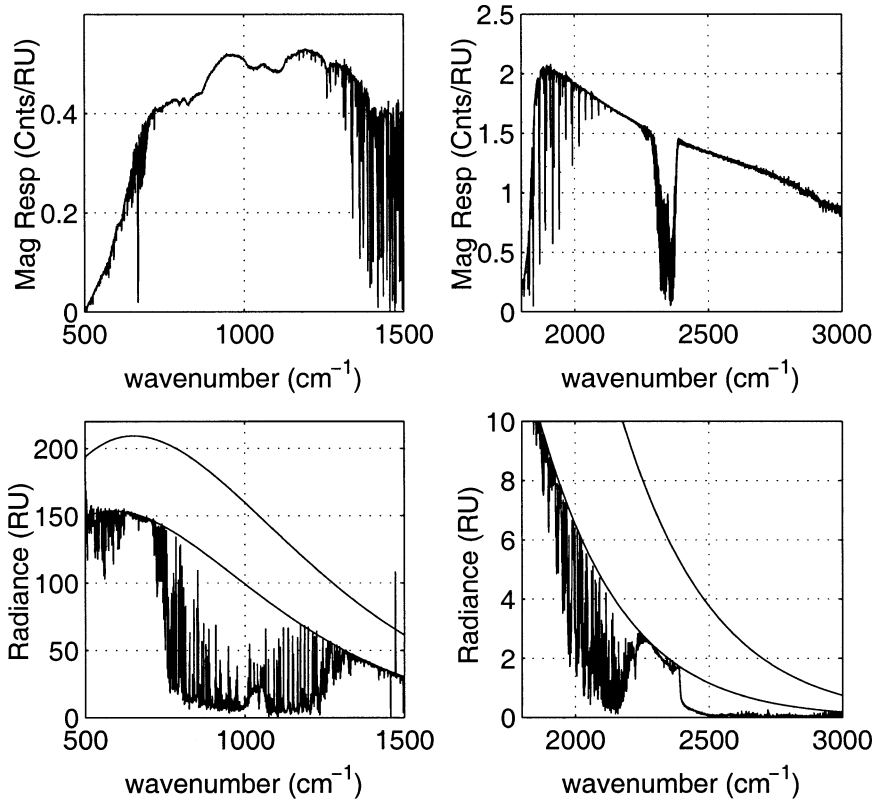

FIG. 3. The (top) responsivity magnitude and (bottom) calibrated radiance spectra for a calibration sequence of AERI-01 from the ARM SGP CF at 0146:21 UTC 18 Sep 2000. The smooth curves in the lower panel correspond to Planck functions at the hot and ambient blackbody temperatures. [Radiance units: RU = mW (m^2 sr cm^{-1})$^{-1}$.]

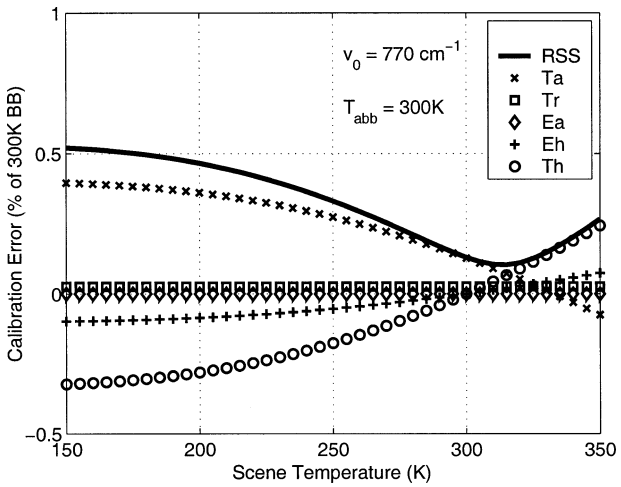

FIG. 4. The predicted 3σ calibration uncertainty for the standard AERI system at 770 cm^{-1} for an ambient blackbody at 300 K and assuming the blackbody uncertainties from Table 3. Separate error estimates are shown for the contribution from the hot blackbody (Th), the ambient blackbody (Ta), the hot blackbody emissivity (Eh), the ambient blackbody emissivity (Ea), and the environment surrounding the blackbodies (Tr). The solid curve is the root sum square (RSS) of the individual contributions.

also shows the combined error for this set of uncertainties as a root sum square of errors. The extrapolation due to the use of a hot blackbody (rather than a cold blackbody) causes the calibration error to increase when the scene temperature is below that of the ambient blackbody. However, the uncertainty analysis shows that the AERI system design will meet the ARM requirement of 1% of ambient radiance if the blackbodies achieve the accuracy defined in Table 3. Moreover, the scene radiance error is reduced as the ambient blackbody temperature decreases. This is particularly important for the Arctic, where the clear-sky scene radiance in the winter is close to zero in the window regions. This analysis suggests that the largest calibration error experienced by the AERI instrument is for hot, dry conditions where

TABLE 3. Parameters used in the AERI calibration uncertainty analysis.

Parameter	Value assumed	Uncertainty estimate (3σ)
T^H	333 K	0.1 K
T^A	Variable	0.1 K
e^H_v	0.996	0.002
e^A_v	0.996	0.002
T^R	Equal to T^A	5

FIG. 5. Typical UW-SSEC laboratory end-to-end calibration verification using reference targets at about 318 (zenith view) and 273.15 K (nadir view). This ''four body'' test was used to verify the radiometric calibration of the AERI instruments prior to deployment of the systems to the DOE ARM sites.

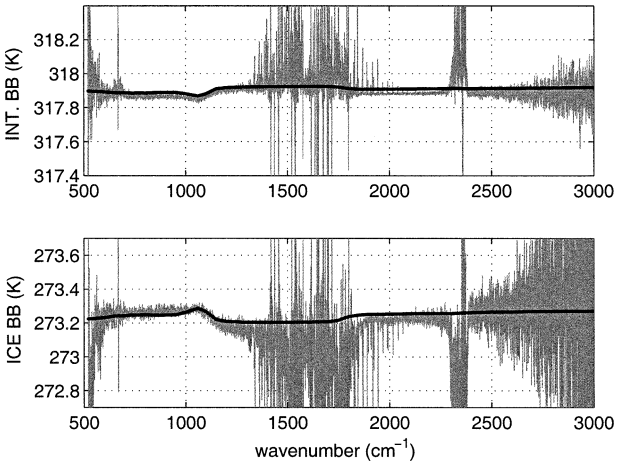

FIG. 6. Laboratory radiometric calibration verification test results for the AERI-06 system conducted at UW-SSEC on 8 May 2001 before deployment to the TWP-Nauru site. (top) The result for the ice blackbody. (bottom) The result for an external blackbody at a temperature ''intermediate'' between the AERI ambient and hot blackbodies. The smooth line is the predicted radiometric temperature based upon the measured blackbody temperatures and the assumed cavity emissivity (cavity factor of 12.79). The measured spectrum is the mean calibrated radiance for the 3.2-h test period converted to equivalent blackbody (brightness) temperature. Strongly absorbing CO_2 and H_2O lines in the air path between the detector and the blackbody reference sources contaminate the measurement between 1400–1900 and 2300–2400 cm^{-1}.

the ambient blackbody temperature is warm but the window radiances are very low. In contrast, the best absolute accuracy (as a percent) is obtained when scenes are close to the ambient blackbody temperature. This is the reason that the Marine-AERI system is able to provide such an accurate measurement of sea surface temperature (Minnett et al. 2001). A detailed analysis of calibration uncertainties of the AERI system under different operating conditions is deferred to a future paper.

(iii) Laboratory radiometric calibration verification

Prior to the deployment of each AERI instrument built for the ARM Program, an end-to-end calibration verification test was performed using UW-SSEC blackbodies as external reference sources. In the laboratory, the AERI hot blackbody is temperature controlled to about 333 K, while the ambient blackbody operates at room temperature (about 300 K). One of the external blackbodies is controlled to an intermediate temperature (about 318 K), while the second external blackbody reference is a cavity partially submerged in an ice slurry bath (273.15 K). The ice temperature cavity is operated with a purge of dry nitrogen to prevent condensation on the interior surfaces during the laboratory tests. The external reference sources are calibrated using the same (National Institute of Standards and Technology) NIST-traceable approach as the AERI onboard blackbody references. Figure 5 shows the typical setup for this ''four body'' test with the intermediate temperature external blackbody in the zenith position and the ice temperature blackbody in the nadir view position. For this test, the scene mirror is programmed to cycle through each of the internal and external blackbody view positions, with a dwell period in each position of about 100. Data are collected in a stable environment over a period of several hours in order to reduce the noise level on the mean measurement. During the test period the temperatures of the external blackbodies are recorded. The external blackbody temperatures are combined with a cavity emissivity model to predict the equivalent blackbody temperature that the AERI instrument should see. The predicted radiometric temperatures for the intermediate and ice blackbody are used as ''truth'' for this test.

An example calibration verification test result from 8 May 2001 for the AERI-06 instrument is shown in Fig. 6. The air path between the interferometer and the reference blackbodies is transparent for most spectral channels, with the exception of the water vapor band (1400–1900 cm^{-1}) and the carbon dioxide bands at 667 cm^{-1} and near 2380 cm^{-1}, which contaminate the measurement. For the standard AERI instruments the signal-to-noise level is also degraded at wavenumbers below about 550 cm^{-1} and above about 2500 cm^{-1}. A wavenumber region in each detector spectral band was chosen to provide an estimate of the error (measured minus predicted) for each calibration verification test. A summary table containing the mean and 1σ uncertainty in

TABLE 4. Summary of AERI laboratory calibration verification results (mK). The mean error and the 1σ uncertainty in the mean is listed for each verification test. The sample mean and sample std dev is computed for the set of seven independent instrument calibration verification tests. The variance among the tests is compared with the 3σ predicted error and the AERI calibration specification (1% of ambient radiance) at the scene temperatures and measured wavelengths.

AERI ID		Intermediate temperature (~318 K)		Ice temperature (~273 K)	
		(900–1100 cm^{-1})	(2100–2200 cm^{-1})	(900–1100 cm^{-1})	(2100–2200 cm^{-1})
02	12 Nov 1998	−47.8 ± 0.4	−37.9 ± 0.1	11.4 ± 0.8	107.6 ± 0.5
03	12 Nov 1998	−4.8 ± 0.2	9.4 ± 0.2	−48.0 ± 0.4	−23.7 ± 0.8
04	9 Dec 1998	0.9 ± 0.8	16.9 ± 0.6	46.9 ± 1.8	67.9 ± 2.8
05	10 Dec 1998	32.4 ± 0.4	29.9 ± 0.7	−61.6 ± 0.8	34.7 ± 3.2
06	1 Jul 1997	0.8 ± 0.2	13.1 ± 0.2	−49.0 ± 0.6	−66.5 ± 1.0
06	8 May 2001	−22.2 ± 0.4	−27.4 ± 0.3	8.9 ± 1.2	−28.5 ± 1.3
08	31 May 2000	36.8 ± 0.4	24.6 ± 0.1	−109.1 ± 0.7	22.9 ± 0.8
Mean		−1	4	−29	16
Std dev		30	26	53	60
3 *std dev		88	79	160	181
Predicted (3σ)		79	83	237	359
1% specification		534	187	828	661

the mean for each instrument test is provided in Table 4. One of the AERI systems (AERI-06) was tested in 1997 and again in 2001; however, the system was completely recalibrated for the test in 2001 with a new detector and new blackbodies, so the two tests are independent from the point of view of radiometric calibration. Variations in the laboratory test results from instrument to instrument provide a measure of the variability in the absolute calibration of the AERI instruments. Table 4 shows the mean and 3σ errors for all the calibration verification tests of the ''standard'' AERI instruments (AERI-02, -03, -04, -05, -06, -08).

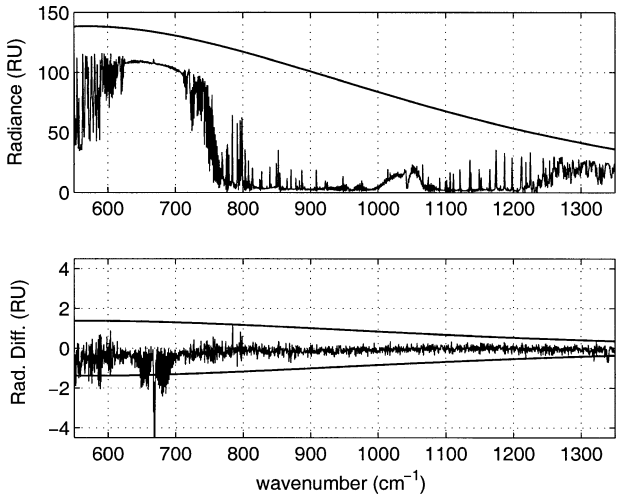

FIG. 7. Coincident clear-sky comparison between AERI-04 (Hillsboro) and the AERI prototype (-00) at UW-SSEC on 7 Dec 1998 at Madison, WI. (top) The overlay of the AERI-04 observed downwelling radiance spectra and a Planck function at the AERI-04 ambient blackbody temperature. (bottom) The radiance difference between AERI-04 and AERI-00 averaged over the 1-h period 1624–1724 UTC. For reference, ±1% of the AERI-04 ambient blackbody radiance is represented by the solid lines. [Radiance units: RU = mW (m^2 sr cm^{-1})$^{-1}$.] See the text for an explanation of the differences in the 660–680-cm^{-1} region.

The measured 3σ errors are compared against a model prediction of the root-mean-square of absolute calibration errors based upon an uncertainty analysis of the calibration equation. This analysis shows that the measured errors are close to the predicted uncertainties at the intermediate body temperature and within the expected error at the ice body temperature. Note that the predicted longwave uncertainty shown in Table 4 is slightly underestimated because it does not include the small contribution due to the uncertainty in the nonlinearity correction. These measurements at the intermediate and ice blackbody temperatures verify the model used to predict the AERI calibration uncertainties at colder scene temperatures. This is further confirmed by the sky intercomparison data presented in the next section.

(iv) Clear-sky radiometric calibration verification

As part of the calibration verification of each AERI instrument prior to initial deployment, a clear-sky intercomparison was performed at UW-SSEC against the AERI prototype instrument (AERI-00). This test was used to verify the radiometric calibration at the cold scene temperatures in the atmospheric window region by comparison to a common reference standard. Each AERI instrument is designed to measure absolute radiance to within 1% of the true ambient blackbody radiance, so the difference of any two instruments should be zero to within the combined uncertainties. Figure 7 shows the intercomparison of the AERI-04 (Hillsboro) instrument with the AERI prototype on 7 December 1998. The difference between the AERI-04 and AERI-00 spectra is actually much better than 1% across the longwave spectral band with one notable exception. The AERI prototype was operating from an enclosure that was warmer than the outside air. This leads to a mismatch with the AERI-04 (which was operating outside) in the most opaque CO_2 and H_2O lines, which are sen-

TABLE 5. Summary of the clear-sky comparison of each AERI system to the AERI prototype at UW-SSEC prior to initial system deployment.

AERI ID		ABB temp	LW B.T.	LW % of ABB radiance (985–990 cm^{-1})	SW B.T.	SW % of ABB radiance (2510–2515 cm^{-1})
02	4 Nov 1998	286.7	161.50	−0.96 ± 0.07	226.41	−0.66 ± 0.25
03	4 Nov 1998	287.6	167.67	−0.14 ± 0.05	226.08	−0.73 ± 0.22
04	7 Dec 1998	289.8	167.97	−0.02 ± 0.04	226.88	−0.06 ± 0.21
05	7 Dec 1998	289.1	167.49	−0.09 ± 0.05	228.11	+0.26 ± 0.28
06	7 July 1997	296.5	194.01	+0.03 ± 0.18	236.18	+0.06 ± 0.14
08	6 Jun 2000	294.0	185.96	−0.79 ± 0.18	237.54	−0.49 ± 0.28
Mean				−0.33		−0.27
Std dev				0.43		0.41

sitive to the air temperature in the first meter of atmosphere above the instrument.

The results from all of the ''pre-ship'' sky intercomparison tests are summarized in Table 5 using narrow window regions near the center of each detector band. The results are presented as a percent of the ambient blackbody radiance of each instrument in order to simplify comparison to expected level of agreement. The largest percentage difference is the longwave AERI-02 minus AERI-00 value of −0.96% (subsequent to this analysis a software calibration parameter was found to be in error for the AERI-02 unit). The mean difference for all of the cases relative to the AERI prototype is about −0.3% in both the longwave and the shortwave bands. Now one can take advantage of the fact that the seven independently calibrated AERI instruments were all compared to the same AERI prototype instrument under similar sky conditions. Assuming that the uncertainties in the absolute calibration of each AERI system vary randomly about the true value, one can interpret the mean error of the set of standard AERI instruments relative to the AERI prototype as an estimate of the absolute calibration error of the AERI prototype instrument. Under this assumption, an estimate of the absolute error of each AERI system at the stated scene temperature can be obtained by subtracting the mean AERI prototype offset from each row of Table 5. The result of including this offset is shown in Fig. 8, which combines the results of the clear-sky intercomparisons in Table 5 with the laboratory calibration verification results of Table 4. Figure 8 suggests that each of the AERI systems built for the ARM Program meet the radiometric calibration specification of 1% of ambient radiance, although the sky intercomparisons cannot preclude an overall systematic error in all instruments. Figure 8 also includes the calibration uncertainty prediction from Fig. 4, assuming an ambient blackbody of 300 K. This prediction does not include the small uncertainty in the longwave band induced by the nonlinearity correction. These results confirm the basic AERI calibration methodology of using high-precision cavity references at hot and ambient temperatures to accurately extrapolate to cold-sky scene temperatures.

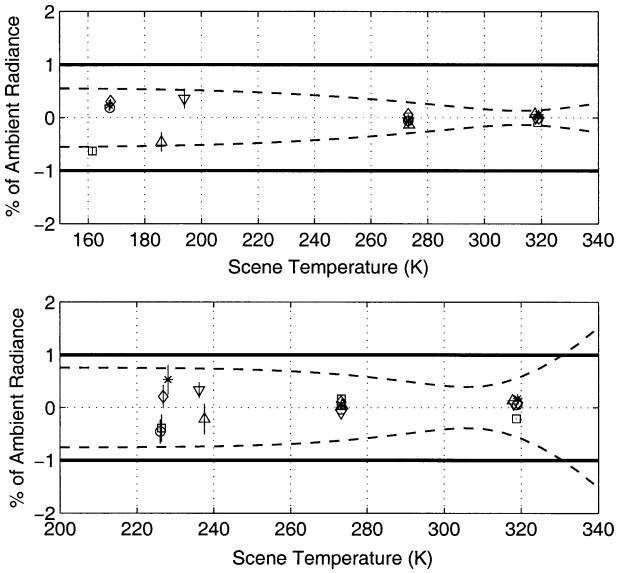

FIG. 8. Verification of the absolute radiometric accuracy of the AERI instruments built by UW-SSEC for the ARM Program showing that each system meets the specification of 1% of ambient radiance. Results are presented for (top) the longwave HgCdTe band near 10 μm and (bottom) the shortwave InSb band near 4 μm. The data points near 318 and 273 K are from the laboratory calibration verification tests using reference blackbodies. The data points at the cold scene temperatures are from clear-sky radiance intercomparisons with the AERI prototype system after the mean AERI prototype bias has been removed. Also shown (dashed curves) is the predicted error (3σ) contribution due to uncertainty in the blackbody parameters only, assuming a 300-K blackbody. The square, circle, diamond, star, downward triangle, and upward triangle represent the AERI-02, -03, -04, -05, -06, and -08 systems, respectively.

3) SPECTRAL COVERAGE AND INSTRUMENT LINE SHAPE

The standard AERI radiance data product is a continuous spectrum between 520 and 3020 cm^{-1} (the requirement is 550–3000 cm^{-1}). The extended-range AERI (ER-AERI) radiance product at the North Slope of Alaska (NSA) site is a continuous spectrum between 380 and 3020 cm^{-1} (the requirement is 400–3000 cm^{-1}). Since the AERI instrument is a Fourier transform spectrometer, the ''unapodized'' spectral resolution is

given by $\Delta\upsilon = 1/(2 \times X)$, where X is the maximum optical path difference (OPD) of the Bomem interferometer. The maximum OPD is defined by the effective sampling frequency of the interferometer laser sampling system and the number of points collected per interferogram. The AERI radiance data product is minimally sampled; that is, the spectral sample frequency is equal to the unapodized spectral resolution.

The real-time AERI radiance product contains a correction for the small effects of instrument self-apodization on the instrument line shape. The correction makes use of the knowledge of the field-of-view (FOV) half-angle to remove the effect of instrument self-apodization in the measured spectrum and create a product that represents an ''ideal'' sinc function instrument line shape. Since the field angles are small, the correction can be made quite accurately. The adjustment of the measured spectrum to that of an ''ideal'' Michelson interferometer on a standard wavenumber grid greatly simplifies the comparison of an AERI observation to radiative transfer calculations or to observations from other coincident AERI instruments. The AERI ''finite field of view'' correction is described here, and the resampling of the spectrum to a standard wavenumber grid is presented in the next section on spectral calibration.

Integration over the angular field of view for an on-axis detector with FOV view half-angle b leads to an equation for the measured interferogram in terms of the source spectrum $S(\upsilon)$ given by

$$I_\upsilon^m(x) = \frac{1}{2\pi}\int d\upsilon e^{i2\pi x\upsilon}\frac{\sin[2\pi x\upsilon(b^2/4)]}{2\pi x\upsilon(b^2/4)}S(\upsilon). \quad (7)$$

Since the FOV half-angle for the AERI systems is small, the sinc function can be expanded in a power series. Substituting for $\mathrm{sinc}(y) = 1 - y^2/3! + y^4/5! + O(y^6)$ in Eq. (7) yields

$$I_\upsilon^m = \frac{1}{2\pi}\int d\upsilon e^{i2\pi x\upsilon}S(\upsilon) \times\left\{1 - \frac{2\pi(b^2/4)]^2}{3!}(x\upsilon)^2 + \frac{[2\pi(b^2/4)]^4}{5!}(x\upsilon)^4 + O\left[\left(\frac{b^2}{4}\right)^6\right]\right\}. \quad (8)$$

If the notation FFT{ } is used to represent the fast Fourier transform, then the measured interferogram including finite-FOV effects can be represented by the true spectrum as

$$I_\upsilon^m = \mathrm{FFT}\{S(\upsilon)\} - \frac{[2\pi(b^2/4)]^2}{3!}x^2\mathrm{FFT}\{\upsilon^2 S(\upsilon)\} + \frac{[2\pi(b^2/4)]^4}{5!}x^4\mathrm{FFT}\{\upsilon^4 S(\upsilon)\} + O\left[\left(\frac{b^2}{4}\right)^6\right]. \quad (9)$$

If the inverse FFT is taken over the measured optical path difference range $[-X_{\max}, +X_{\max}]$ of each term in Eq. (9), a formula is obtained that approximates the measured spectrum as a convergent power series in the parameter b^2. Substituting the measured spectrum for the true spectrum in the power series, the correction to the measured spectrum, ΔC_υ^m, can be solved for in terms of the measured spectrum as

$$\Delta C_\upsilon^m \cong \frac{[2\pi(b^2/4)]^2}{3!}\mathrm{FFT}^{-1}\{x^2\mathrm{FFT}\{\upsilon^2 C_\upsilon^m\}\} - \frac{[2\pi(b^2/4)]^4}{5!}\mathrm{FFT}^{-1}\{x^4\mathrm{FFT}\{\upsilon^4 C_\upsilon^m\}\}. \quad (10)$$

The correction defined by Eq. (10) has been implemented as a power series where the calibrated spectrum is scaled by υ^n, an FFT is performed, and the interferogram multiplied by x^n before applying an inverse FFT to return to the spectral domain. Figure 9 shows the magnitude of the first term in the finite FOV correction. The second term in Eq. (10) is more than two orders of magnitude below the first term in the correction and far below the instrument noise level.

4) SPECTRAL CALIBRATION

The wavenumber calibration of an FTS system is determined by the interferogram sampling interval in optical path delay. The MR100 interferometer used in the AERI system is a continuous-scan interferometer using laser fringe detection to trigger the sampling of the infrared detectors. A complete double-sided interferogram is recorded for each detector band without the use of numerical filtering. The wavenumber scale corresponding to an AERI detector band is given by the formula $\upsilon = (i - 1)\Delta\upsilon$, for $i = 1$, $N_{\mathrm{DS}}/2$, and $\Delta\upsilon = \upsilon_{\mathrm{eff}}/N_{\mathrm{DS}}$, where υ_{eff} is the effective sampling frequency and N_{DS} is the number of points in the double-sided interferogram. The MR100 acquisition software records a power-of-two number of points based upon a mechanical switch setting. The AERI system uses the MR100 in the highest-spectral-resolution mode, where N_{DS} equals 32 768. The actual interferogram sampling frequency is the laser frequency modified by the effect of integration over a finite angular field of view. The effective sampling frequency is

$$\upsilon_{\mathrm{eff}} \cong \upsilon_{\mathrm{laser}}(1 + b^2/4), \quad (11)$$

where $\upsilon_{\mathrm{laser}}$ is the laser frequency and b is the half-angle of the interferometer field of view. The half-angle b for the AERI instruments is known by design. For the AERI-01 system, $b = 16$ mrad, which gives an effective laser sampling frequency of 15 799.03 cm^{-1} for a nominal HeNe laser frequency of 15 798.02 cm^{-1}. However, angular misalignment between the infrared and laser optical paths through the interferometer can introduce an additional effective frequency shift beyond that given by Eq. (11). To account for any small alignment imperfections, the effective sampling frequency υ_{eff} is determined empirically for each detector of each AERI

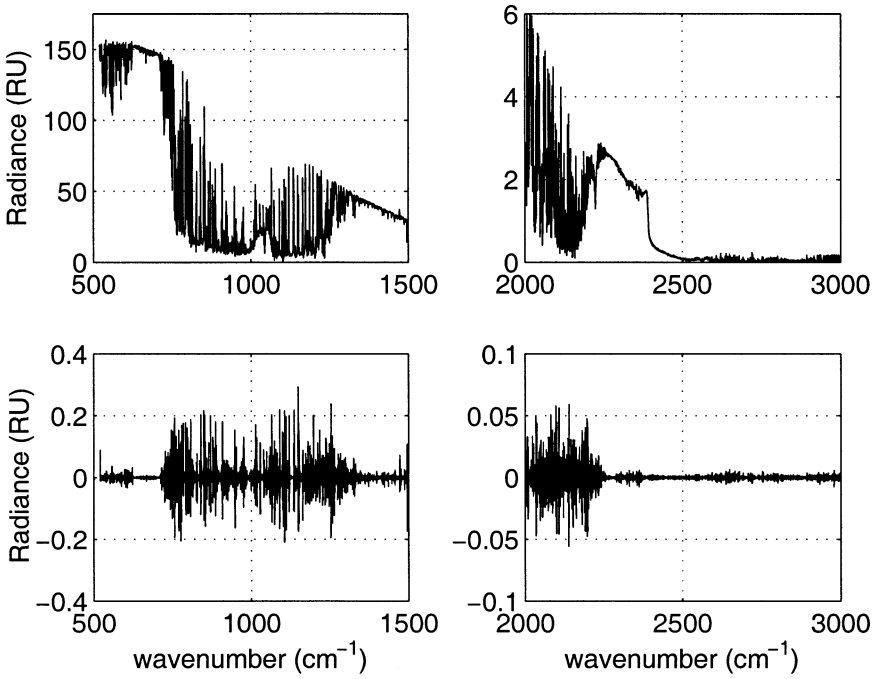

FIG. 9. (bottom) Finite-FOV correction for (top) an AERI-01 radiance observation from the ARM SGP CF at 0146:21 UTC 18 Sep 2000. [Radiance units: RU = mW (m² sr cm⁻¹)⁻¹.]

system prior to deployment in the field. Subsequent analysis of field observations can also be used to further refine this initial spectral calibration.

The approach to wavenumber calibration of the AERI instruments is to take advantage of gaseous line center positions known to high accuracy through laboratory measurements (Rothman et al. 1992). A line-by-line radiative transfer model (LBLRTM) is used to calculate a downwelling atmospheric emission spectrum using a radiosonde profile of temperature and water vapor coincident with an AERI observation. The effective sampling frequency υ_{eff} is determined empirically by minimizing the standard deviation between observed and calculated emission spectra as the effective sampling frequency of the observation is varied. This minimization is illustrated in Fig. 10 for the regularly spaced CO_2 lines in the wavenumber range 730–740 cm^{-1}. A similar analysis is performed in the AERI shortwave band using the regularly spaced N_2O lines between 2207 and 2220 cm^{-1}. Prior to the initial deployment of each AERI system, a clear-sky observation of downwelling radiance was recorded coincident with a radiosonde launched from UW-SSEC. The LBLRTM was used with a version of the HITRAN database to calculate the downwelling emission at the surface (Clough and Iacono 1995; Rothman et al. 1992). Uncertainties in the atmospheric water vapor and temperature profiles cause the minimum in the standard deviation shown in Fig. 10 to be nonzero; however, this introduces only a small error in the determination of the effective sampling frequency. The AERI spectral calibration requirement is stated in Part I as ''better than 0.01 cm^{-1}'' over the entire spectral range. At 3020 cm^{-1}, the 0.01-cm^{-1} requirement translates into a knowledge of $\Delta\upsilon$, and hence υ_{eff}, of 3.3 ppm (or better).

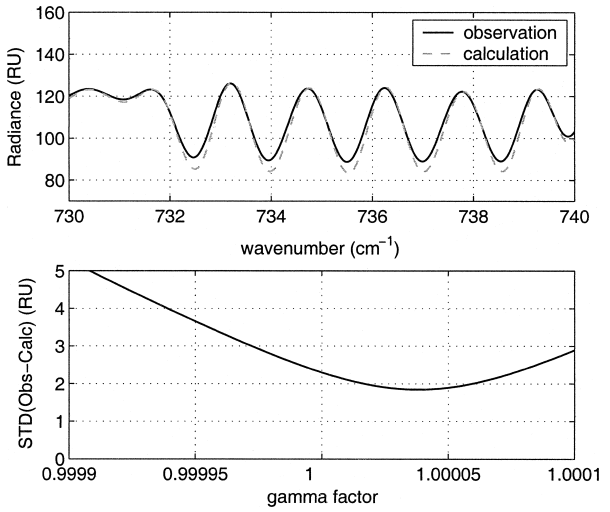

FIG. 10. The AERI longwave effective sampling frequency, υ_{eff}, is determined by the wavenumber scale factor that minimizes the std dev of the difference between observation and calculation for the wavenumber region 730–740 cm^{-1}. The gamma factor is the ratio of the adjusted wavenumber scale to a reference wavenumber scale. Example is from the AERI-01 at the ARM SGP CF at 1120 UTC 30 Sep 2001. [Radiance units: RU = mW (m² sr cm^{-1})$^{-1}$.]

A detailed analysis was performed to quantify the uncertainty in this spectral calibration technique and to

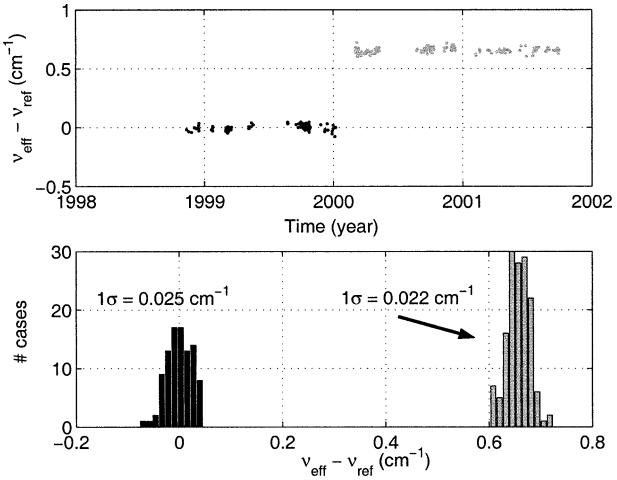

FIG. 11. (top) The time series of $\upsilon_{\text{eff}} - \upsilon_{\text{ref}}$ for each of the 142 cases of AERI-01 longwave observations and clear-sky calculations based upon microwave-scaled radisondes launched from the ARM SGP CF. The wavenumber reference for this figure (15 798.74 cm^{-1}) is the mean of the 95 cases prior to Feb 2000. The abrupt change after Feb 2000 was due to the replacement of the instrument laser. (bottom) The same data plotted as a histogram. These results demonstrate an ability to determine the AERI spectral calibration to an accuracy of 1.5 ppm (1σ) using atmospheric observations.

assess the long-term stability of the AERI spectral calibration. A fit to the effective sampling frequency of the AERI-01 system was performed using 241 cases of clear-sky AERI observations coincident with radiosonde launches at the DOE ARM SGP Central Facility. The data span the period from 11 November 1998 to 30 September 2001 (35 months). The calculations were performed using LBLRTM v6.01 with HITRAN2000. The radiosonde (Vaisala RS80-H) water vapor profiles were scaled to agree with the total precipitable water column measured by a coincident microwave radiometer (standard ARM processing). The details of this set of clear-sky observations is described in Turner et al. (2004). In February 2000, the HeNe laser in the AERI-01 system was replaced, presumably changing the relative alignment of the laser and the infrared beam. The upper panel of Fig. 11 clearly shows the abrupt change in the longwave effective sampling frequency caused by the laser replacement in what otherwise is a very stable spectral calibration. The data fall into two groups: 95 cases before January 2000 and 146 cases after the laser replacement in February 2000. A statistical analysis of the AERI-01 longwave spectral calibration has been performed on the two sets. The AERI-01 longwave band effective laser sampling frequency determined before initial deployment of the AERI-01 system (in 1995) was 15 798.80 cm^{-1}, with an estimated uncertainty of about 0.05 cm^{-1}. The refined analysis using the 95 coincident radiosonde cases at the ARM SGP Central Facility prior to January 2000 gives a mean value of 15 798.74 cm^{-1}, with a 1σ standard deviation of 0.025 cm^{-1}, that is, 1.6 ppm. The analysis using the 145 cases between March 2000 and September 2001 gives a new mean value for the period after the laser change of 15 799.40 cm^{-1}, with a 1σ value of 0.022 cm^{-1}, that is, 1.4 ppm. A similar analysis has been performed on the shortwave AERI spectral band using the wavenumber region 2207–2220 cm^{-1}. The AERI-01 shortwave band effective laser sampling frequency determined before initial deployment of the AERI-01 system (in 1995) was 15 798.62 cm^{-1}, with an estimated uncertainty of about 0.05 cm^{-1}. The analysis of the shortwave band prior to January 2000 gives the same mean value of 15 798.62 cm^{-1} but with a 1σ standard deviation of 0.015 cm^{-1} out of 15 799 cm^{-1}, that is, 0.95 ppm. After January 2000, the shortwave mean value was determined to be 15 799.21 cm^{-1}, with a 1σ standard deviation of 0.021 cm^{-1}, that is, 1.3 ppm, after the laser replacement. In summary, the wavenumber knowledge determined from a single AERI/radiosonde comparison during the initial instrument testing before deployment should be accurate to within about 3 ppm (2σ), with 95% confidence, which meets the AERI specification. However, this analysis shows that the uncertainty in the wavenumber scale of each AERI system can be further reduced (by at least an order of magnitude) by careful comparison with a large set of coincident clear-sky radiative transfer calculations, as was demonstrated for the AERI-01 system.

Once the spectral calibration is known, the AERI radiance spectrum can be resampled from the ''original'' sampling interval to a standard ''reference'' wavenumber scale. The reference wavenumber scale for all of the AERI instruments was chosen to correspond to an effective laser sampling frequency of 15 799.0 (exact). The resampling is performed in software using an FFT, ''zero padding,'' and linear interpolation of an oversampled spectrum. This procedure is numerically intensive but can be performed without loss of accuracy. The advantage of providing the AERI radiance product on a standard wavenumber scale is to simplify comparison with radiative transfer model calculations and with other AERI instruments.

5) NOISE

The AERI requirement on radiometric noise performance is stated as a standard deviation of observed radiance during a 2-min dwell of a hot blackbody (+60°C) over a specified wavenumber range. A separate specification is used for the longwave band of the ER-AERI. The horizontal lines in Fig. 12 show the AERI noise specification found in Part I. Note that while the ER-AERI achieves enhanced noise performance out to 425 cm^{-1}, the noise performance from 600 to 1400 cm^{-1} is degraded relative to the standard AERI detectors. For this reason, a standard AERI system is preferred over an ER-AERI system for all but the driest atmospheres when the 380–500-cm^{-1} rotational water vapor band becomes important.

In order to continuously monitor the AERI instrument

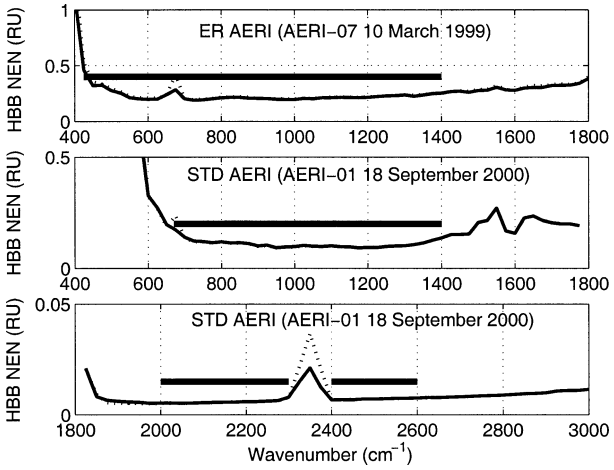

FIG. 12. The noise specification on the hot blackbody reference view for the longwave band of (top) an ER-AERI, (middle) the longwave band of a standard AERI, and (bottom) the shortwave band of any AERI, shown with horizontal solid lines. The two curves (solid and dotted) are the hot blackbody noise estimate from the two real-time AERI noise products. The two noise estimates agree so well that the curves fall directly on top of each other. [Radiance units: RU = mW (m^2 sr cm^{-1})$^{-1}$.]

noise performance, the real-time AERI software was designed to generate two data products that estimate the actual noise performance. The first AERI noise estimate uses the variance computed during the dwell period of the internal hot blackbody reference. The equation for the first AERI noise estimate is

$$\text{HBB\_NEN1} = \langle \sigma_H^F \rangle_{25\,\text{cm}^{-1}} \left(\frac{1}{2}\right) \sqrt{\frac{\text{DwellTime}}{2\ \text{min}}}, \quad (12)$$

where σ is the square root of the variance of magnitude spectra collected during the forward Michelson sweep directions of the hot blackbody view. The average is the mean over 25-cm^{-1} wavenumber bins across the spectrum. The time ratio accounts for the difference between the actual dwell time and the 2-min period called out in the specification. The factor of one-half accounts for the fact that the measured variance is of the complex magnitude rather than the real part and that the variance is only from the forward direction Michelson scans, whereas the mean spectrum is the average of forward and backward scans. The second hot blackbody noise estimate computes a wavenumber standard deviation over 25-cm^{-1} regions of the real part of the difference between hot blackbody complex spectra collected at the start ($H1$) and end ($H2$) of each calibration sequence. The count values are converted to radiance using the 25-cm^{-1} average responsivity corresponding to that calibration sequence. The equation for the second AERI noise estimate can be written as

$$\text{HBB\_NEN2} = \text{STD}_\nu(\text{Re}\{C_\nu^{H1} - C_\nu^{H2}\})_{25\,\text{cm}^{-1}} \left(\frac{1}{\langle \Re_\nu \rangle_{25\,\text{cm}^{-1}}}\right), \quad (13)$$

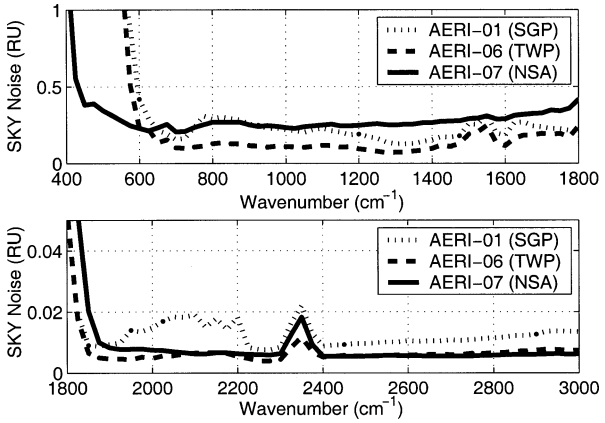

FIG. 13. Noise on three calibrated clear-sky scenes observed by the AERI. The curves show the real-time sky noise product from the AERI-01 system at the SGP CF on 18 Sep 2000, the AERI-06 instrument at the TWP-Nauru site on 15 Nov 1998, and the ER-AERI (-07) at the NSA-Barrow site on 10 Mar 1999. [Radiance units: RU = mW (m^2 sr cm^{-1})$^{-1}$.]

where STD represents the standard deviation. Under normal operating conditions, the two AERI noise estimates are in good agreement with each other. Figure 12 illustrates the two noise estimates for both a standard and an extended-range AERI instrument.

The real-time AERI software also produces an estimate of the noise on the final calibrated scene. This estimate makes use of the imaginary part of the calibration equation given in Eq. (5). A 25-cm^{-1} wavenumber standard deviation is performed on the imaginary part corresponding to each scene. The ''forward'' Michelson mirror scans are used to make the estimate so the result is divided by $\sqrt{2}$ to estimate the noise on the final scene (average of forward and backward scans). Figure 13 shows an example of the ''sky'' noise product for an AERI scene from each of the three ARM sites (SGP, NSA, and TWP). The increase in the AERI-01 noise level in the atmospheric window is due to the contribution of noise from the hot and ambient reference sources caused by the calibration extrapolation to low scene radiances (Sromovsky 2003).

6) REPRODUCIBILITY

The short-term reproducibility of the AERI observations is illustrated in Fig. 14 with a time series of observations of an external UW-SSEC blackbody at 318 K for the AERI-03 (Vici) instrument. The test was the same setup shown in Fig. 5 and summarized in Table 4. In order to study the time variation of the calibration, the random noise was reduced by a factor of 20 using spectral averages in three 200-cm^{-1} regions of the longwave spectrum. The peak-to-peak variation of observed brightness temperature is less than ± 5 mK relative to the mean over the 4-h period, which corresponds to a peak-to-peak radiance variation of less than 0.01% at 1000 cm^{-1}. This exceptional stability is a result of the

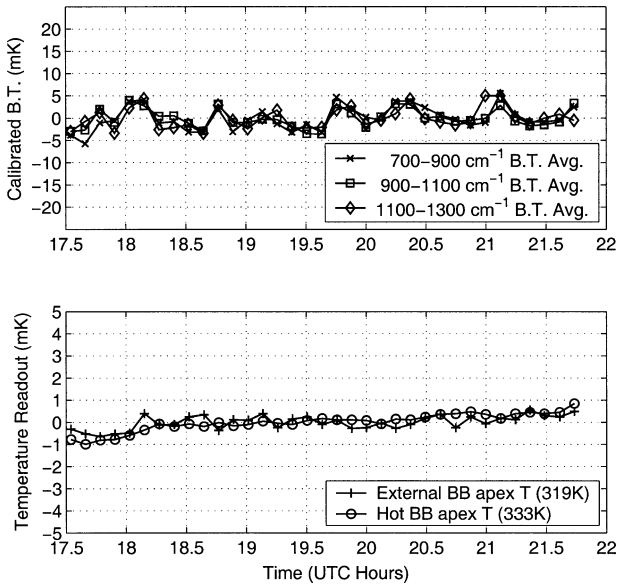

FIG. 14. (top) Short-term calibration reproducibility of better than 5 mK and (bottom) temperature control better than 1 mK, illustrated using a blackbody target at 318K. Data were collected from the AERI-03 (Vici) instrument at UW-SSEC on 12 Nov 1998. This performance exceeds the ARM requirement for calibration reproducibility by an order of magnitude.

long time constant of the AERI blackbodies and the excellent blackbody temperature control and readout precision. The lower panel of Fig. 14 shows that the short-term temperature control of the AERI blackbodies is better than ± 1 mK (peak to peak) relative to the mean over the test period. The AERI short-term reproducibility is well within the ARM requirement of 0.2%.

3. Conclusions

The performance of the AERI instruments designed and built at UW-SSEC meet the ARM Program requirements for downwelling infrared spectral observations at the surface. The AERI instruments built for the ARM Program have demonstrated radiometric accuracy of better than 1% of ambient radiance, with a reproducibility of better than 0.2%. A routine correction for nonlinearity of the longwave HgCdTe detector is applied to the observed data in real time. A small correction for instrument line shape is also applied to create an idealized ''sinc'' line shape function, and the data are resampled onto a standard wavenumber grid for convenience in comparison to model calculations. The spectral calibration is known to better than 1.5 ppm (1σ) using known spectral positions of atmospheric lines. A comprehensive error analysis of the AERI observations for tropical, midlatitude, and Arctic environments is the subject of a future paper.

Acknowledgments. This research was supported by the Office of Science (BER), U.S. Department of Energy, Grants DE-FG02-90ER61057 and DE-FG02-92ER61365. Special thanks go to Dave Turner of Pacific Northwest National Laboratory for his encouragement during the writing of this paper.

REFERENCES

Clough, S. A., and M. J. Iacono, 1995: Line-by-line calculations of atmospheric fluxes and cooling rates. 2: Applications to carbon dioxide, ozone, methane, nitrous oxide and the halocarbons. *J. Geophys. Res.*, **100,** 16 519–16 535.

Knuteson, R. O., and Coauthors, 2004: Atmospheric Emitted Radiance Interferometer. Part I: Instrument design. *J. Atmos. Oceanic Technol.,* **21,** 1763–1776.

Minnett, P. J., R. O. Knuteson, F. A. Best, B. J. Osborne, J. A. Hanafin, and O. B. Brown, 2001: The Marine-Atmospheric Emitted Radiance Interferometer (M-AERI), a high-accuracy, sea-going infrared spectroradiometer. *J. Atmos. Oceanic Technol.,* **18,** 994–1013.

Revercomb, H. E., H. Buijs, H. B. Howell, D. D. LaPorte, W. L. Smith, and L. A. Sromovsky, 1988: Radiometric calibration of IR Fourier transform spectrometers: Solution to a problem with the High-Resolution Interferometer Sounder. *Appl. Opt.,* **27,** 3210–3218.

Rothman, L. S., and Coauthors, 1992: The HITRAN molecular database: Editions of 1991 and 1992. *J. Quant. Spectrosc. Radiat. Transfer,* **48,** 469–507.

Sromovsky, L. A., 2003: Radiometric errors in complex Fourier transform spectrometry. *Appl. Opt.,* **42,** 1779–1787.

Stokes, G. M., and S. E. Schwartz, 1994: The Atmospheric Radiation Measurement (ARM) Program: Programmatic background and design of the Cloud and Radiation Testbed. *Bull. Amer. Meteor. Soc.,* **75,** 1201–1221.

Turner, D. D., and Coauthors, 2004: The QME AERI LBLRTM: A closure experiment for downwelling high spectral resolution infrared radiance. *J. Atmos. Sci.,* **61,** 2657–2675.